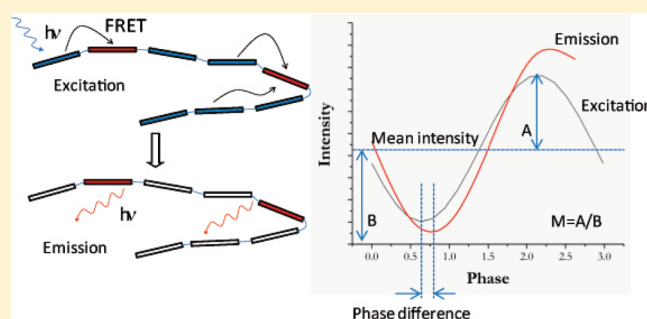


## Electronic Energy Transfer in Highly Aligned MEH-PPV Single Chains

Matthew C. Traub,<sup>†</sup> Girish Lakhwani,<sup>†,||</sup> Joshua C. Bolinger,<sup>†</sup> David Vanden Bout,<sup>\*,§</sup> and Paul F. Barbara<sup>†,‡</sup><sup>†</sup>Center for Nano and Molecular Science and Technology and <sup>§</sup>Department of Chemistry and Biochemistry, University of Texas, Austin, Texas 78712, United States

S Supporting Information

**ABSTRACT:** This paper describes the simultaneous measurement of excitation and emission anisotropy to visualize energy transfer in single chains of the prototypical conjugated polymer MEH-PPV, for samples with >70% of the single chains organized into extended, rod-like conformations. The uniformity and high degree of order of the single molecules in these experiments has allowed direct comparison of our experimental data to energy-transfer simulations in model polymer chains. Increases in average anisotropy from 0.62 to 0.74 from excitation to emission and average changes of <15° to the in-plane dipole principal orientation axis confirmed that energy was transferred to a relatively small number of sites in these highly ordered chains. This organization persisted even at large molecular weights ( $M_n = 850$  kDa). Electronic energy transfer in highly anisotropic model chains was simulated using an incoherent Förster-type mechanism to generate modulation depth histograms in good agreement with the observed data, as well as ensemble emission energies consistent with previously reported results. In these ordered model chains, excitons migrated an average of 6 nm before emission. This distance, far larger than the radius for single-step FRET, implies that energy transfer in MEH-PPV is a multistep funneling process.



## INTRODUCTION

While it is widely accepted that electronic energy transfer (EET) in conjugated polymers (CPs) is intimately connected to their morphology,<sup>1–5</sup> a direct determination of their relationship has not been possible with ensemble measurements of inherently heterogeneous films. Spatially averaged ensemble measurements of these complex materials simultaneously probe multiple morphological domains of unknown structure, limiting their ability to provide insight into structure/function correlations. However, in a single-molecule fluorescence experiment, each diffraction-limited spot contains a single nanodomain whose properties can be independently interrogated, allowing quantitative treatment of energy transfer in a well-defined morphological environment. Our group has previously explored conformation in single-polymer chains of MEH-PPV by using fluorescence excitation polarization spectroscopy to measure the anisotropy,  $A_{ex}$ , of these single nanodomains and relating these observed anisotropies to simulated molecular conformations.<sup>6</sup> While the original experiments showed a broad distribution of anisotropies (and corresponding morphologies), recent experiments with improved quality samples containing a lower number of tetrahedral defects have shown that the vast majority of the chains (>70%) are organized into highly polarized structures ( $A_{ex} > 0.6$ ).<sup>7,8</sup> Thus, this system presents an opportunity to study energy transfer in a largely uniform, organized environment.

Rapid EET of excitons between segments in single CP molecules was first postulated based on MEH-PPV emission

spectra.<sup>9</sup> Spectrally resolved fluorescence microscopy has shown that there is a bimodal distribution of emission energies in MEH-PPV single molecules, with an ensemble emission spectrum composed of spectrally distinct “red” and “blue” peaks ( $\lambda_{max} = \sim 585$  and 545 nm, respectively, at 300 K).<sup>10–14</sup> The ensemble emission spectrum is independent of excitation wavelength,<sup>11</sup> consistent with efficient EET from all segments of the chain to a relatively small number of emitting chromophores.

These observations are in stark contrast to emission of MEH-PPV in solution or in bulk films. The ensemble solution emission spectrum consists of a single peak with  $\lambda_{max} = 550–560$  nm,<sup>15,16</sup> while the emission of the bulk film is dominated by a single peak at  $\sim 585$  nm.<sup>17,18</sup> This difference has been postulated to occur because of formation of and efficient energy trapping by “red sites” in bulk materials.<sup>19</sup> In addition to the bathochromic shift in the emission spectrum, trapping by red sites limits the range of exciton diffusion in amorphous films of MEH-PPV to 5–10 nm.<sup>20</sup> However, recent experiments have shown that in highly ordered single molecules, energy can transfer from excitons to polarons over distances of 50 nm or more,<sup>21</sup> emphasizing the importance of understanding morphology to controlling bulk behavior.

The source of the bimodal distribution of chromophore energies and the range and efficiency of EET to red sites are major outstanding scientific questions that cannot be addressed without

Received: May 17, 2011

Published: August 04, 2011

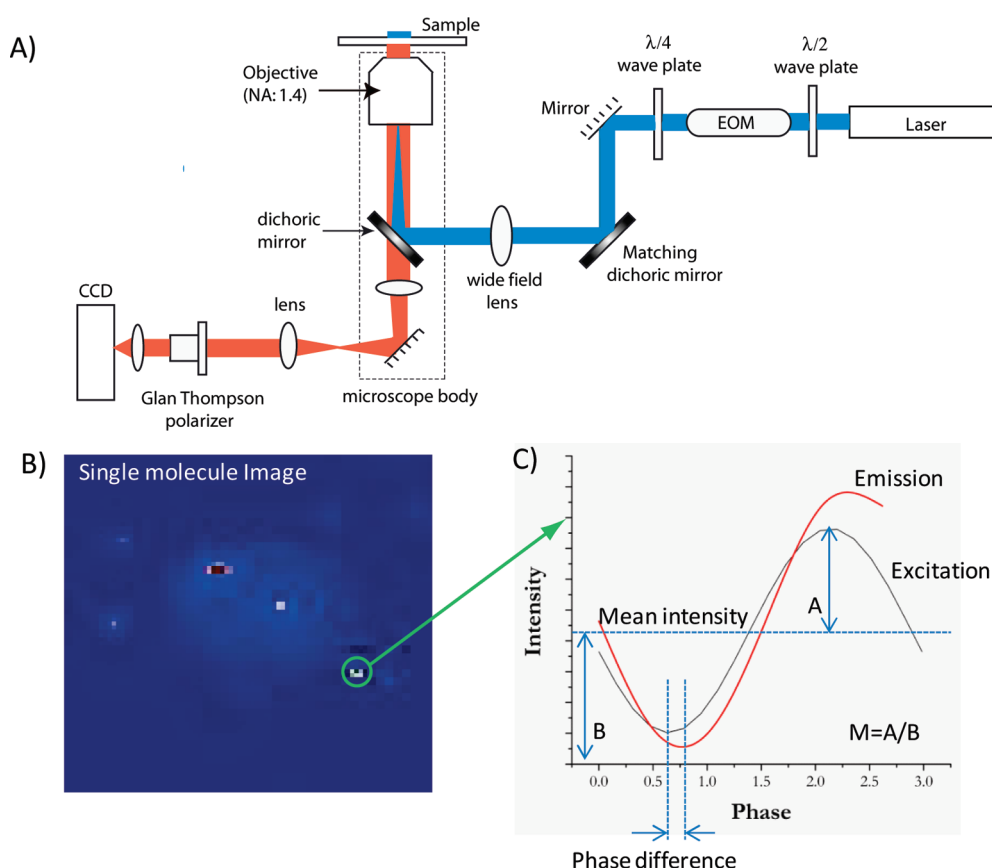


**Figure 1.** (A) The experimental setup for excitation/emission correlation experiments. An electro-optic modulator rotated the phase angle of the linearly polarized excitation beam. Emitted light passed through a polarizer mounted on a rotation stage to an EM-CCD. Full excitation transients were collected at emission polarizer angles of  $0, \pi/6, \pi/3, \pi/2, 2\pi/3$ , and  $5\pi/6$ . (B) A wide-field single-molecule image of MEH-PPV obtained on the experimental apparatus. (C) Full excitation and emission transients obtained by averaging excitation measurements over all emission or excitation polarizer angles, respectively. The modulation depth ( $M$ ) and in-plane dipole orientation phase difference are illustrated.

understanding the polymers' conformation. To this end, we have visualized energy transfer in MEH-PPV by simultaneously measuring the fluorescence excitation and emission polarization of single molecules that are known to have highly ordered chain conformations. The polarized excitation light democratically probes all absorbing chromophores that contribute to fluorescence, providing for each molecule both a modulation depth ( $M_{\text{ex}}$ , corresponding to molecular anisotropy, as described below) and an in-plane dipole principal orientation axis. To examine EET, we also probe the polarized emission of the same single molecule. Polarized detection of emission provides a corresponding modulation depth ( $M_{\text{em}}$ ) and in-plane dipole orientation of only the subset of chromophores that are emitting (Figure 1).

To extract more quantitative information on EET in single MEH-PPV chains, we simulated experimentally observed histograms and previously reported emission spectra using a Förster resonance energy-transfer (FRET) model. The molecular anisotropy and in-plane dipole orientation angle of model MEH-PPV chains were simulated,<sup>6,7</sup> and energy was allowed to migrate through these model chains by a Förster-type mechanism. We found that successful simulation of all of the experimental data simultaneously requires multistep energy funneling to a small ( $<3\%$ ) number of chromophores in a highly aligned chain. These results clearly demonstrate that even in the limit of FRET, the high organization of the conjugated polymer leads to ET across the entire polymer chain.

## EXPERIMENTAL SECTION

**Materials.** Poly[2-methoxy-5-(2'-ethyloxy)]-1,4-phenylenevinylene (MEH-PPV) was purchased from Polymer Source. MEH-PPV of a number average molecular weight ( $M_n$ ) of 150 kg/mol (PDI = 3.0) was used as received. MEH-PPV with a listed  $M_n$  of 2600 kg/mol was purified by GPC (Viscotek VE 2001), yielding a sample with  $M_n$  = 850 kg/mol (PDI = 3.0). Poly[methyl methacrylate] (PMMA,  $M_n$  = 45 kg/mol) was purchased from Sigma-Aldrich. Anhydrous toluene (99.8%, Acros) was used to prepare all samples.

**Samples.** Samples were fabricated on glass coverslips (Fisher). All coverslips were rinsed with acetone, cleaned of fluorescent impurities by immersion in a solution of  $\text{H}_2\text{O}_2/\text{H}_2\text{SO}_4$  (piranha etch), rinsed with nanopure water ( $>18 \text{ M}\Omega$ ), and dried with  $\text{N}_2$ . [Caution: Piranha etch is aggressive and explosive. Never mix piranha waste with organic solvents. Check precautions before using it.]

All samples were prepared in an inert atmosphere glovebox. Single-molecule concentrations of MEH-PPV were prepared in 6 wt % solutions of PMMA in toluene. The solutions were dynamically spin coated onto the coverslips at 2000 rpm, yielding 200 nm films of PMMA embedded with single MEH-PPV molecules. Samples were packaged in the glovebox using epoxy and a coverslip to prevent photobleaching of molecules by ambient  $\text{O}_2$ .

**Experimental Apparatus.** Studies were performed using an apparatus designed to simultaneously modulate excitation and emission polarization (Figure 1). The 488 nm line of an Ar ion laser (Melles Griot, 35-IMA-040-208) was passed through a Glan-Thompson polarizer, a half-wave plate, a low-voltage electro-optic modulator (Fastpulse), and a quarter wave plate. The voltage across the EOM was controlled by a high-voltage power supply (Trek, model 50/750) driven by a programmable function generator (Wavetek, model 29A), providing control over the phase angle of the linearly polarized excitation. The excitation was passed through a lens ( $f = 300$  mm) located outside of an inverted confocal microscope (Zeiss, Axiovert 100), filtered (488 interference filter, CVI), and focused into the back of the microscope objective (Zeiss, 100 $\times$  ApoPlano 1.4 NA). To compensate for the polarization-angle-dependent reflectivity of the dichroic mirror, light was reflected off of a matched dichroic mirror before entering the microscope. Excitation scatter was filtered through a dichroic mirror and filter (488 nm notch, Semrock). Emitted fluorescence was collimated with a doublet lens, passed through a Glan-Thompson polarizer (Newport) mounted on a computer-controlled rotation stage (Newport NSR-1), and focused through a doublet lens onto a Peltier-cooled EM-CCD (Andor iXon). The angle between the incident polarization and the emission analyzer was calibrated using 240 nm diameter isotropic fluorescent beads (SpheroTek).

To collect a data set, the emission polarizer was held at a fixed angle, and the phase angle of the excitation light was continuously rotated from 0 to  $\pi$ . For each area, this procedure was repeated for emission polarizer angles of 0,  $\pi/6$ ,  $\pi/3$ ,  $\pi/2$ ,  $2\pi/3$ , and  $5\pi/6$ . Data were processed using home-built Matlab software. Excitation and emission transients for individual molecules were fit using a procedure described previously.<sup>6,7</sup>

**Energy-Transfer Simulations.** Model polymer conformations were generated using Monte Carlo simulations of a stiff conjugated polymer chain from coarse-grain beads on a chain model. The details of the coarse-grain polymer chain simulations and their resulting conformations have been reported previously.<sup>6,7</sup> EET within these conformations is simulated using the segments between the beads to model the polymer chromophores. We simulate FRET between individual chromophores in each polymer chain using a Pauli master equation (eq 1), where  $P(t)$  is the probability of energy being at chromophore  $i$  at time  $t$ .<sup>22</sup>

$$\dot{P}(t) = W^T \cdot P(t) \quad (1)$$

$$W = [t_{ij}]_{z \times z} \quad (2)$$

$$t_{ij} = (\chi_{ij})^2 \frac{9(\ln 10)J_{ij}}{128\pi^5 n^4 N_A} \frac{\phi}{\tau} \frac{1}{r_{ij}^6} \quad \text{for } i \neq j \neq z$$

$$t_{ij} = - \sum_{\substack{m=1 \\ m \neq n \\ n=i}}^z t_{im} \quad \text{for } i = j \neq z$$

$$t_{iz} = k_{nr} \quad t_{zj} = 0 \quad (3)$$

where  $t_{ij}$  is the rate of energy transfer from the  $i$ th chromophore to the  $j$ th chromophore, whose separation, spectral overlap and orientation factors are  $r_{ij}$ ,  $J_{ij}$ , and  $\chi_{ij}$ , respectively. In this expression,  $n$  is the refractive index,  $N_A$  is Avogadro's number,  $\phi$  is the quantum yield of fluorescence in the absence

of an acceptor,  $\tau$  is the associated lifetime, and  $k_{nr}$  is the nonradiative decay rate. In this simulation,  $\phi$ ,  $\tau$ , and  $k_{nr}$  are assumed to be the same for all chromophores with  $\phi = 0.2$ .<sup>23</sup> The diagonal terms ( $i = j$ ) are the sum of all decay paths out of that chromophore site. Finally, there is an additional column included in the matrix,  $t_{iz}$ , that accounts for the loss due to nonradiative decay.

The polymer chains are composed of 200 beads ( $z - 1$  chromophores), with a distance between two consecutive beads corresponding to 2.5 monomer units. Each vector connecting two consecutive beads is treated as a single chromophore, whose dipole moment orientation and center of mass are given by the vector's direction and midpoint, respectively. Hence, the distance between each pair of donor–acceptor chromophores,  $r_{ij}$ , is given by

$$r_{ij} = |\vec{r}_i - \vec{r}_j| \quad (4)$$

with an associated orientation  $\chi_{ij}$  given by

$$\chi_{ij} = \cos \alpha_{ij} - 3 \cos \beta_{ij} \cos \gamma_{ij} \quad (5)$$

where  $\alpha_{ij}$  is the angle between the dipole moments of the donor and acceptor chromophores and  $\beta_{ij}$  and  $\gamma_{ij}$  are the angles between the dipole moments of the chromophores and the vector joining them.

The absorbance spectrum,  $\varepsilon_j$  of each chromophore was simulated using a log-normal energy distribution, with a resonance (mean) energy chosen randomly from a bi-Gaussian energy distribution,  $G$ . The mean energies of this distribution were 20 500  $\text{cm}^{-1}$  for the main peak and 17 500  $\text{cm}^{-1}$  for a second low-energy peak. The fraction of the overall distribution comprised of the low-energy peak was varied as described below. The parameters used for the log-normal distribution are chosen to match the absorbance of a chromophore to the experimentally observed absorption of phenylene–vinylene oligomers.<sup>15,24</sup> The corresponding emission spectrum,  $F_i$  was calculated by assuming that it was a mirror image of its absorbance spectrum displaced by a constant Stokes shift of 600  $\text{cm}^{-1}$ .

Using the above parameters, eq 6 yields the probability  $P(t)$  of energy being at each chromophore at time  $t$

$$P(t) = \sum_{j=1}^z c_j e^{a_j t} m_j \quad (6)$$

where  $a$  are the eigenvalues,  $m$  is the corresponding eigenvectors (each  $z \times 1$  dimension), and  $c$  are the corresponding coefficients. The coefficients  $c$  can be calculated using eq 7

$$c_j = [M^{-1}P(0)]_j \quad (7)$$

$M$  is the  $z \times z$  matrix containing  $z$  eigencolumn vectors and  $P(0)$  is the starting probability of energy being at any specific chromophore at time  $t = 0$ . Using the rate constant of fluorescence,  $k_f$  of the chromophores, the respective emission yields can be calculated using eq 8

$$Y_j = k_f m_j \int_0^\infty e^{a_j t} dt = \frac{k_f m_j}{-a_j} \quad (8)$$

The initial probabilities used to solve eq 1 are derived from the overlap between the excitation wavelength and the absorption spectrum of each chromophore. The absorption tensor of each conformation is generated from the incoherent sum of chromophores weighted by their initial population. Similarly,



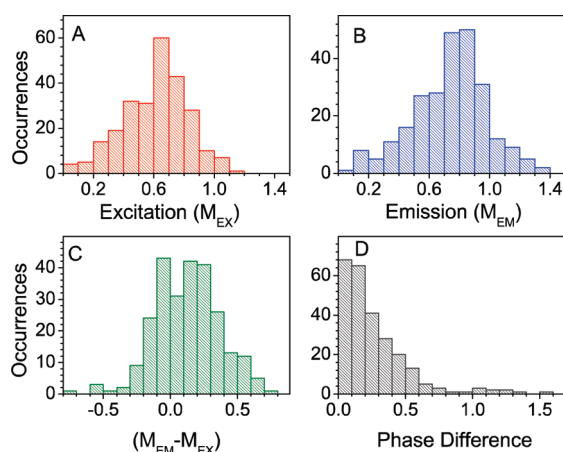


**Figure 2.** Histogram of observed modulation depths for (A) excitation and (B) emission for 150k MEH-PPV single molecules. (C) Change in anisotropy from excitation to emission for each molecule. (D) In-plane dipole orientation phase angle difference between excitation and emission.

the emission tensors were generated from the incoherent sum of the chromophores weighted by their final emission yields. Simulated absorption and emission modulation depths were generated by taking the in-plane projection of the absorption and emission tensors and accounting for the depolarizing effects of the high numerical aperture objective.<sup>25,26</sup>

An ensemble histogram of single-molecule emission peak energies was also simulated from the energies and final probabilities of all chromophores summed over all conformations considered. For these simulations, the fraction of total chromophore energies randomly drawn from the low-energy Gaussian centered at 17500 cm<sup>-1</sup> was 0, 2.5, and 4.25%.

## RESULTS AND DISCUSSION

**Polarization Modulation Depth and Dipole Orientation Histograms.** The modulation depth of each synchronized excitation and emission intensity transient as a function of polarization angle  $\theta$  was fit to the equation

$$I(\theta) \propto 1 + M \cos 2(\theta - \phi) \quad (9)$$

where  $\phi$  is the angle where the emission intensity is maximized.

The excitation modulation depth  $M_{\text{ex}}$  is the  $x$ - $y$  plane projection of the molecular absorption tensor  $A_{\text{ex}}$  which reflects the overall shape of the molecule, as described below. The distribution of tilt angles in the molecular frame means that the observed  $M_{\text{ex}}$  for a given molecule provides a lower bound on its true anisotropy (i.e., a high  $A_{\text{ex}}$  can lead to a low observed  $M_{\text{ex}}$  for a molecule tilted far out of the  $x$ - $y$  plane). The observed mean and standard deviation of 0.62 and 0.21 for  $M_{\text{ex}}$  (Figure 2A) are nearly identical to the recently reported values of 0.66 and 0.22 for an  $M_n$  of 150K.<sup>7</sup> When these identical samples were measured without the emission polarizer, the previous narrower histograms were duplicated. We attribute the slightly lower value observed here to a decreased signal-to-noise ratio due to the additional polarizer rather than any change in the properties of the samples themselves. As has been shown previously,<sup>7</sup> when the effects of molecular tilt angle and depolarization by the high numerical aperture objective are accounted for, the mean excitation anisotropy is  $\sim 0.75$ . This high value can only be explained by assigning an extended, rod-like conformation to the majority of

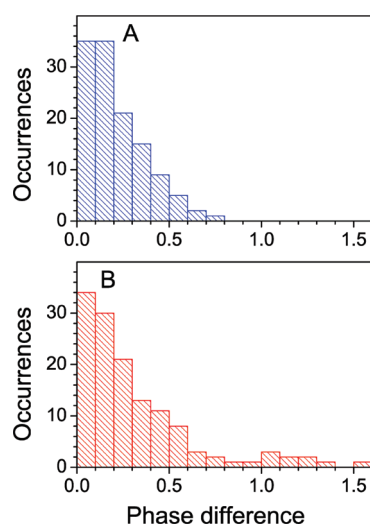


**Figure 3.** Distribution of the phase angle difference for single molecules of MEH-PPV ( $M_W = 150k$ ) obtained for (a) above and (b) below  $M_{\text{ex}} = 0.65$ .

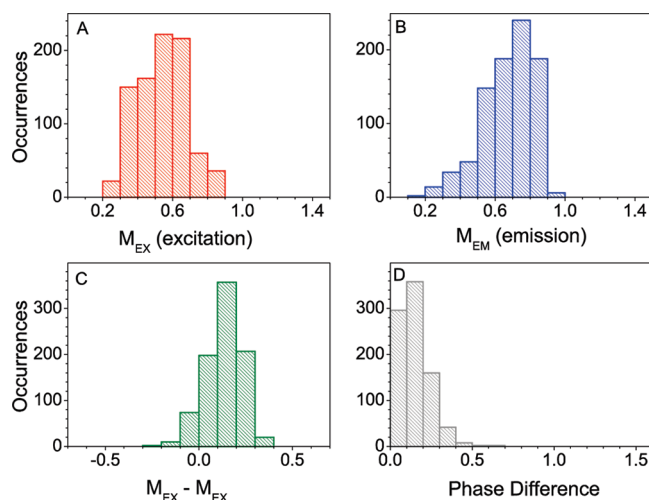


**Figure 4.** Simulated histogram of observed modulation depths for (A) excitation and (B) emission for the 150k MEH-PPV single molecules. (C) Change in anisotropy from excitation to emission for each molecule. (D) In-plane dipole orientation phase angle difference between excitation and emission.

the single CP chains in the sample. The angle  $\phi$  is the orientation of the in-plane dipole principal orientation axis (and its corresponding absorption tensor) or essentially the orientation of the long axis of each rod-like chain in the  $x$ - $y$  sample plane. The spin-coating process randomly orients each molecule, and values of  $\phi$  for excitation are evenly distributed from 0 to  $\pi$ .

Excitation at 488 nm, near the peak of the solution absorption band, probes all of the chromophores whose absorptions contribute to the total fluorescence of the molecule, providing data on the overall shape of the molecule. In contrast, fitting the emission transient for each molecule measures the alignment and orientation solely of the subset of chromophores that subsequently emit and can be used to extract information on energy transfer in the polymer. It should be noted that any chromophores that are completely quenched before emitting or transferring energy to another emissive chromophore will not

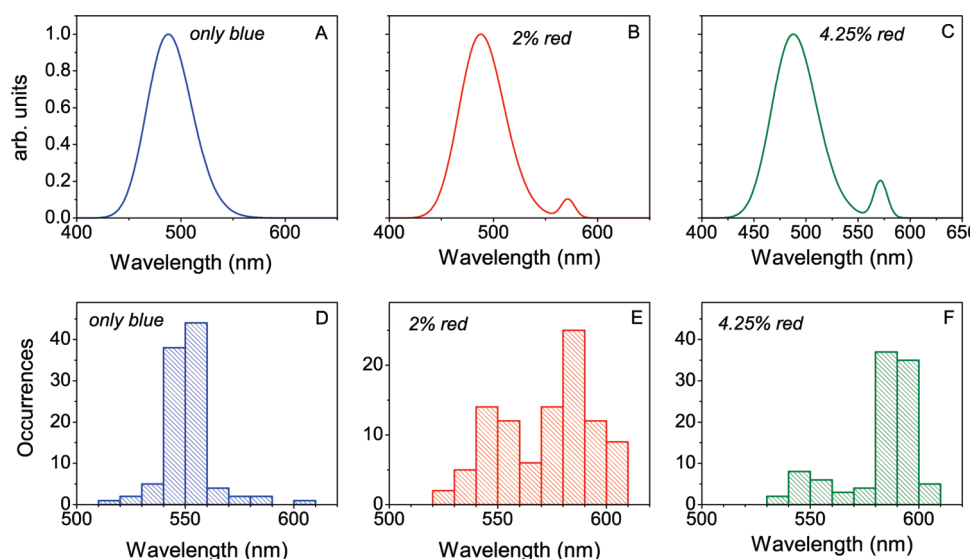


**Figure 5.** The bi-Gaussian energy distribution (with peaks at wavelengths 488 [blue] and 570 nm [red]) inputs given to model 150k MEH-PPV single chains for FRET simulations containing (A) only blue sites, (B) 2% red sites, and (C) 4.25% red sites. (D–F) Respective histograms for the peak position of single-molecule emission energies obtained from the FRET simulations.

be visualized by either experiment, and “dark”, completely nonemissive regions cannot be ruled out by these experiments.

The effects of energy transfer on emission anisotropy can be illustrated by considering limiting cases. In the total absence of energy transfer, the observed modulation depths for absorption and emission will be essentially identical, while if there is complete energy funneling to a single chromophore, the emission anisotropy will be unity. An example of the latter was observed by Lupton and co-workers for a short-chain polyindeno-fluorene end-capped with a perylene acceptor, which measured an increase in modulation depth from a peak of 0.45 in excitation to  $\sim 1$  in emission due to energy transfer to the single dipole end cap.<sup>27</sup> As shown in Figure 2B, the histogram of emission anisotropy had both a higher mean (0.74) and a narrower width than that for excitation. The distribution of changes in anisotropy (Figure 2C) shows that while anisotropy can decrease for a given chain, the majority of molecules show an increase or little change. Given the already high mean value of  $M_{\text{ex}}$ , the narrow, high-peak value histogram observed for emission is not surprising and is consistent with energy transfer to a subset of chromophores in an organized molecule.

The change in in-plane dipole orientation from excitation to emission can also be used to confirm our picture of CP conformation. For highly ordered, rod-like chains, nearly all of the chromophores have the same in-plane orientation, and energy transfer to any particular subset of chromophores should yield little change in  $\phi$ . In contrast, energy transfer to selected sites in a more disordered molecule will yield a broader dispersion of orientation angles, and energy transfer from a single dipole to an orthogonal one would yield the maximum change of  $\pi$ . As seen in Figure 2D, the majority of dipole orientation shifts are clustered below 0.4, with a mean of  $<0.25$ . To confirm that larger orientation shifts were not from the fraction of the sample assigned to the rod-like structure, we sorted observed orientation shifts by their corresponding  $M_{\text{ex}}$  and found that all of the larger values observed were due to chains with  $M_{\text{ex}} < 0.65$ . (Figure 3) Additionally, a histogram of phase differences between different molecules ( $\phi_{\text{em},1}$ ,  $\phi_{\text{ex},2}$ , etc.) (Figure S1, Supporting Infor-

mation) showed no correlation, ruling out phase selection in our experimental apparatus as the source of our low measured shifts. The overall order of the chain was very insensitive to increases in the molecular weight of the sample. Measurement of the  $M_w = 850$  K sample showed nearly identical values for the mean  $M_{\text{ex}}$ ,  $M_{\text{em}}$ , and dipole orientation shift (0.60, 0.66, and 0.23 respectively). (Figure S2, Supporting Information)

**Simulated Histograms and Emission Energies.** There have been some previous measurements of the excitation and emission anisotropy in MEH-PPV,<sup>28,29</sup> but in these experiments, the observed excitation modulation depths were more broadly dispersed than those in the current study. Moreover, these studies did not take into account either an explicit model for the polymer conformation or its orientation in the lab frame and thus provide limited physical insight. To extract a quantitative picture of energy transfer in single molecules, we have simulated histograms of the excitation and emission modulation depth using model beads-on-a-chain polymers. This approach includes an explicit model for the chain conformations and energy distributions and allows us to apply more physically valid models of chromophore emission than previous speculation about so-called “emitting sites”. Additionally, this approach accounts for experimental effects, including the tilt angle of the molecules in the laboratory frame and polarization distortion by the high NA objective.

The histograms in Figure 4 show the results of simulations resulting from a single Gaussian distribution of initial energies (centered at 488 nm with a bandwidth of 50 nm). The mean of the simulated excitation modulation depth histogram is similar to that observed experimentally (0.57 versus 0.62). The distribution of modulation depths in the simulated histogram is substantially narrower, and there is a complete absence of values below 0.25 (Figure 4A), indicating that we are only examining a well-ordered subset of the total single-chain conformations. Consistent with this, the simulated changes in the in-plane dipole orientation phase have a lower mean than those observed experimentally (0.08 versus 0.26), with no values above 0.3 radians (Figure 4d). After energy transfer to low-energy sites in the Gaussian

distribution, a majority of the emission occurs from a relatively small fraction of the chain, on average,  $\sim 10$  chromophores. As a result, there is an average increase of 0.13 in modulation depth from excitation to emission.

To correctly reproduce the single-molecule ensemble emission peak energies, we selected the energies of a small fraction of the chromophores from a second, bathochromically shifted Gaussian distribution. The simulated histograms of ensemble emission peak energies as a function of the fraction of the total chromophores designated as red are shown in Figure 5. While using a distribution without these red sites reproduced only the blue molecules of the bimodal emission peak distribution (Figure 5A), assigning more than 3% of the chromophores as red sites resulted in only the red peak (Figure 5C). To reproduce the appropriate ratio of red-to-blue molecules ( $\sim 2:1$  at 300 K for excitation at 488 or 514 nm),<sup>11,30</sup> we assigned red energies to 1–3% of the total chromophores. For a 200 bead chain, this resulted in an average of 2–6 red sites per chain, each of which could efficiently receive energy over long distances. These results are consistent with recent results from Basché and co-workers,<sup>30</sup> who observed red emission and high excitation anisotropy upon direct excitation of red chromophores with  $\lambda_{\text{ex}} \geq 568$  nm. We note that the choice of which chromophores to designate red was made randomly and has no bearing on the (unknown) physical source of their bathochromic shift. The introduction of these red sites produced negligible changes on the simulated emission modulation depth histogram.

By combining the final quantum yield for each chromophore  $j$  for excitation at chromophore  $i$  (eq 8) with a distance  $r_{ij}$  between them, we calculate that excitons migrate an average of 6.2 nm from excitation to emission. This distance is several times longer than the single-step FRET radius in MEH-PPV ( $\sim 2$  nm) and confirms the importance of multistep energy funneling in modeling energy transfer in conjugated polymers. Additionally, it should be emphasized that this probably represents a lower bound on the actual diffusion of the excitons. The relatively short length of the chromophore segments in our model chains (2.5 monomers) means that we must use a point-dipole approximation for our energy-transfer calculation. For transition dipoles closer to the expected average chromophore length in the actual chains ( $>10$  monomers), the length of the transition dipoles becomes substantially larger than the nearest-neighbor distances, and a line-dipole approximation becomes more appropriate.<sup>1,31</sup> Additionally, recent demonstrations of coherence across multiple chromophore segments in MEH-PPV at room temperature<sup>32</sup> suggest that a coherent transport model could lead to longer exciton migration distances. Previous theoretical studies of coherent transport in single MEH-PPV molecules showed exciton diffusion limited by chain disorder,<sup>33,34</sup> and a re-examination of this mechanism in highly ordered structures would be very informative for understanding longer-range energy migration processes.

## CONCLUSIONS AND SUMMARY

We simultaneously measured the excitation and emission anisotropy of single chains of the conjugated polymer MEH-PPV in a PMMA matrix. An average observed modulation depth of 0.62 in excitation, corresponding to an anisotropy of  $\sim 0.75$  and a highly extended rod-like conformation, was observed, in agreement with previous results. Small in-plane dipole orientation shifts and an average increase of 0.12 in observed

emission modulation depth are consistent with energy transfer to a small subset of sites within the highly aligned chain. We were able to successfully simulate our observed histograms and previously published ensemble emission data by modeling exciton migration using an incoherent Förster mechanism for energy transfer within explicit chain conformations. Even in the absence of distinct red sites in the chain, efficient long-range multistep energy transfer results in emission from only the lowest-energy sites in the overall distribution of chromophores. To correctly simulate the single-molecule ensemble emission spectrum, we introduced a small number of ( $<3\%$ ) of red sites to the chromophore distribution. Inclusion of greater numbers produced only the red portion of the bimodal emission spectrum, demonstrating the ability of red sites to harvest and trap energy over long distances in highly ordered polymer nanodomains.

## ASSOCIATED CONTENT

**S Supporting Information.** Experimental results for high molecular weight samples and controls. This material is available free of charge via the Internet at <http://pubs.acs.org>.

## AUTHOR INFORMATION

### Corresponding Author

\*E-mail: [dvandenbout@mail.utexas.edu](mailto:dvandenbout@mail.utexas.edu).

### Notes

<sup>†</sup>Professor Barbara passed away in October, 2010.

### Current Addresses

<sup>||</sup>Department of Physics, Cavendish Laboratory, University of Cambridge, J. J. Thomson Avenue, Cambridge, United Kingdom.

## ACKNOWLEDGMENT

We acknowledge funding by the U.S. Department of Energy Basic Energy Sciences, Solar Photochemistry Program (ER15746), and the Robert A. Welch Foundation (F-0020). We gratefully thank Dr. Johanna Brazard for the GPC fractionation of MEH-PPV samples, and Takuji Adachi for helpful discussions.

## REFERENCES

- (1) Scholes, G. D. *Annu. Rev. Phys. Chem.* **2003**, *54*, 57–87.
- (2) Hoffmann, S. T.; Scheler, E.; Koenen, J. M.; Forster, M.; Scherf, U.; Strohhriegel, P.; Bassler, H.; Kohler, A. *Phys. Rev. B* **2010**, *81*, 165208.
- (3) Ma, W. L.; Yang, C. Y.; Gong, X.; Lee, K.; Heeger, A. J. *Adv. Funct. Mater.* **2005**, *15*, 1617–1622.
- (4) Bredas, J. L.; Beljonne, D.; Coropceanu, V.; Cornil, J. *Chem. Rev.* **2004**, *104*, 4971–5003.
- (5) Lupton, J. M. *Adv. Mater.* **2010**, *22*, 1689–1721.
- (6) Hu, D. H.; Yu, J.; Wong, K.; Bagchi, B.; Rossky, P. J.; Barbara, P. F. *Nature* **2000**, *405*, 1030–1033.
- (7) Adachi, T.; Brazard, J.; Chokshi, P.; Bolinger, J. C.; Ganesan, V.; Barbara, P. F. *J. Phys. Chem. C* **2010**, *114*, 20896–20902.
- (8) Habuchi, S.; Onda, S.; Vacha, M. *Phys. Chem. Chem. Phys.* **2011**, *13*, 1743–1753.
- (9) Heun, S.; Mahr, R. F.; Greiner, A.; Lemmer, U.; Baessler, H.; Halliday, D. A.; Bradley, D. D. C.; Burn, P. L.; Holmes, A. B. *J. Phys.: Condens. Matter* **1993**, *5*, 247–60.
- (10) Kim, D. Y.; Grey, J. K.; Barbara, P. F. *Synth. Met.* **2006**, *156*, 336–345.
- (11) Lee, Y. J.; Kim, D. Y.; Grey, J. K.; Barbara, P. F. *ChemPhysChem* **2005**, *6*, 2404–2409.

- (12) Yu, J.; Hu, D.; Barbara, P. F. *Science* **2000**, 289, 1327–1330.
- (13) Ebihara, Y.; Habuchi, S.; Vacha, M. *Chem. Lett.* **2009**, 38, 1094–1095.
- (14) Feist, F. A.; Basche, T. *J. Phys. Chem. B* **2008**, 112, 9700–9708.
- (15) Chang, R.; Hsu, J. H.; Fann, W. S.; Liang, K. K.; Chang, C. H.; Hayashi, M.; Yu, J.; Lin, S. H.; Chang, E. C.; Chuang, K. R.; Chen, S. A. *Chem. Phys. Lett.* **2000**, 317, 142–152.
- (16) Padmanaban, G.; Ramakrishnan, S. *J. Am. Chem. Soc.* **2000**, 122, 2244–2251.
- (17) Gaab, K. M.; Bardeen, C. J. *J. Phys. Chem. B* **2004**, 108, 4619–4626.
- (18) Nguyen, T.-Q.; Martini, I. B.; Liu, J.; Schwartz, B. J. *J. Phys. Chem. B* **2000**, 104, 237–255.
- (19) Yakimov, A. V.; Savvate'ev, V. N.; Davidov, D. *Synth. Met.* **2000**, 115, 51–56.
- (20) Lewis, A. J.; Ruseckas, A.; Gaudin, O. P. M.; Webster, G. R.; Burn, P. L.; Samuel, I. D. W. *Org. Electron.* **2006**, 7, 452–456.
- (21) Bolinger, J. C.; Traub, M. C.; Adachi, T.; Barbara, P. F. *Science* **2011**, 331, 565–567.
- (22) Grage, M. M. L.; Pullerits, T.; Ruseckas, A.; Theander, M.; Inganas, O.; Sundstrom, V. *Chem. Phys. Lett.* **2001**, 339, 96–102.
- (23) Samuel, I. D. W.; Crystall, B.; Rumbles, G.; Burn, P. L.; Holmes, A. B.; Friend, R. H. *Chem. Phys. Lett.* **1993**, 213, 472–478.
- (24) Gierschner, J.; Cornil, J.; Egelhaaf, H. J. *Adv. Mater.* **2007**, 19, 173–191.
- (25) Forkey, J. N.; Quinlan, M. E.; Goldman, Y. E. *Prog. Biophys. Mol. Biol.* **2000**, 74, 1–35.
- (26) Axelrod, D. *Methods Cell Biol.* **1989**, 30, 333–352.
- (27) Becker, K.; Lupton, J. M. *J. Am. Chem. Soc.* **2006**, 128, 6468–6479.
- (28) Lin, H.; Tabaei, S. R.; Thomsson, D.; Mirzov, O.; Larsson, P.-O.; Scheblykin, I. G. *J. Am. Chem. Soc.* **2008**, 130, 7042–7051.
- (29) Mirzov, O.; Bloem, R.; Hania, P. R.; Thomsson, D.; Lin, H. Z.; Scheblykin, I. G. *Small* **2009**, 5, 1877–1888.
- (30) Feist, F. A.; Zickler, M. F.; Basché, T. *ChemPhysChem* **2011**, 12, 1499–1508.
- (31) Westenhoff, S.; Daniel, C.; Friend, R. H.; Silva, C.; Sundstroem, V.; Yartsev, A. J. *Chem. Phys.* **2005**, 122, 094903/1–094903/8.
- (32) Collini, E.; Scholes, G. D. *Science* **2009**, 323, 369–373.
- (33) Dykstra, T. E.; Hennebicq, E.; Beljonne, D.; Gierschner, J.; Claudio, G.; Bittner, E. R.; Knoester, J.; Scholes, G. D. *J. Phys. Chem. B* **2009**, 113, 656–667.
- (34) Singh, J.; Bittner, E. R.; Beljonne, D.; Scholes, G. D. *J. Chem. Phys.* **2009**, 131.